

# APPLICATION OF ELECTROSLAG STRIP CLADDING FOR REACTORS IN HYDROGEN-BASED REFINERY SERVICE

Mitul Patel<sup>a</sup>, R. H. Madnani<sup>a</sup>, B. J. Chauhan<sup>b</sup> and S. Sundaresan<sup>b</sup>

<sup>a</sup> *Larsen & Toubro Ltd., HED Ranoli Works,*

*101, GIDC, Ranoli, Dist:Vadodara, Gujarat.*

<sup>b</sup> *Asst.. Professor. and L & T Welding Chair, Dept. of Met. & Matls. Engg.,*

*M .S. University, Vadodara*

## Abstract

For internal protection of hydroprocessing reactors from high-temperature environmental effects, it is necessary to deposit austenitic stainless steel weld overlays on carbon steel or low-alloy steel base materials. Among the many overlaying possibilities for large-size reactors, submerged and electroslag strip cladding have emerged as primary candidates. Recent reports have shown that the electroslag cladding process offers superior joint quality and is also more cost-effective. The current paper describes the work done for establishing process parameters for electroslag strip cladding in the fabrication of reactors for hydrogen service. The work involved depositing austenitic stainless steel weld overlays (309L/347) on a 1.25Cr-0.5Mo low-alloy steel base metal. In addition to establishing appropriate overlay and PWHT procedures, the work also involved detailed microstructural characterization. The results of quality assessment tests such as NDE, bend testing and IGC testing satisfied all acceptance criteria. Autoclave testing for hydrogen disbanding susceptibility also confirmed the total absence of any disbonded area. Preliminary indications are that even single-layer overlays might provide acceptable reactor service, if their reliability can be further established.

*Key words* : Electroslag cladding, structural changes, hydrogen disbonding

## Introduction

All hydroprocessing reactors need to be internally protected from high-temperature corrosion effects or hydrogen attack. Economic factors as a rule do not permit fabricating the components from solid high-alloyed materials. As a consequence, it is necessary to deposit stainless steel weld overlays such as type 347 on the low-alloy steel base materials. The overlay welding in heavy-wall pressure vessels is commonly carried out using strip electrodes and the two most productive systems for surfacing large components are submerged arc strip cladding (SASC) and electroslag strip cladding (ESSC) [1].

Among the most important factors affecting the economy and metallurgical integrity of any clad surface are deposition rate and degree of dilution [2]. Both SASC and ESSC are characterized by a high deposition rate and low dilution, as well as a high deposit quality [1, 3]. Although until the early 1990s high deposition rate cladding was performed almost exclusively by SASC, subsequent work has demonstrated that ESSC could produce an even higher deposition rate, lower dilution and lower inclusion content in comparison to SASC [4]. In addition, ESSC has been shown to be more cost-effective and hence single-layer electroslag strip cladding tends to be more frequently used than double-layer procedures with submerged arc strip cladding [1].

In ESSC (Fig.1), a strip electrode is continuously fed into a shallow layer of electrically conductive flux. The heat required to melt the strip, the slag-forming flux and the surface layer of the base metal is generated by resistance heating due to the welding current flowing through the molten conductive slag. In relation to submerged-arc strip cladding, the penetration and hence the dilution are reduced in electroslag strip cladding because of the absence of the arc, typical dilution levels lying between 10-15% [1]. The use of a conductive slag and resistance heating instead of an electric arc permits higher current densities to be used in ESSC without increasing penetration. Thus deposition rates higher than that possible with SASC can be achieved in ESSC without increasing the degree of dilution [5, 6]. The flux used in ESSC contains, in addition to oxides like TiO<sub>2</sub> and FeO, a large quantity of

fluorides such as  $\text{CaF}_2$  and  $\text{NaF}$  in order to achieve the required electrical conductivity [5]. The high  $\text{CaF}_2$  content in flux has been shown to decrease dilution level [2], and also reduce the oxygen content in the deposited cladding to a level which is just one third compared to submerged arc surfacing [4]. Furthermore, the solidification rate of the electroslag weld metal is lower, facilitating the escape of gases and the rise of slag particles to the surface. This reduces porosity and inclusion content.

One of the problems in electroslag strip cladding is undercutting, resulting from the electromagnetic pinch effect as the high welding current flows from the strip electrode through the molten pool to the ground cable connected to the base metal. The electromagnetic force in the weld pool generates a flow of molten slag and metal from the sides to the centre of the bead, resulting in undercutting. These forces are usually counteracted, and undercutting prevented, by applying an external magnetic field through a magnetic steering device generating forces in the opposite direction [5, 7].

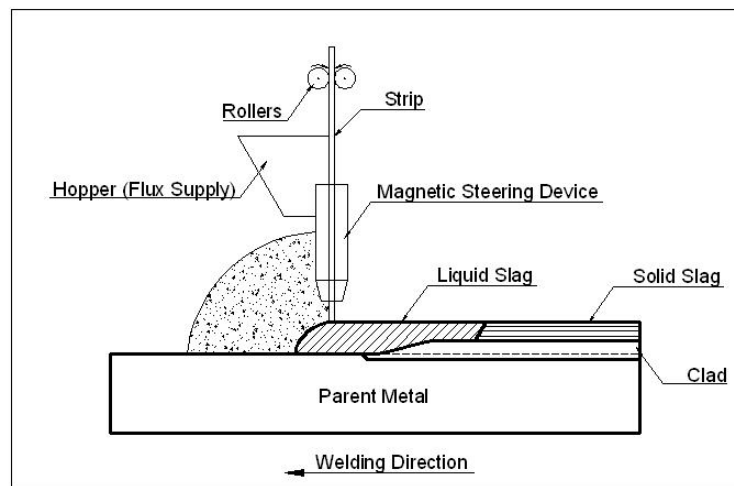


**Fig 1 :** Schematic diagram of the ESSC process

Cladding or dissimilar metal welds sometimes exhibit unique cracking phenomena not observed in welds between similar materials. One such problem is the cracking or disbonding along or near the fusion boundary in dissimilar ferritic-austenitic welds [8]. Such cracking has the potential to cause cladding failures requiring much expenditure in repair or replacement. Although the exact mechanism of disbonding is not completely known, it is believed to occur as a result of hydrogen embrittlement. During the operation of the reactor, atomic hydrogen diffuses into the reactor wall leading to a higher concentration in the austenitic overlay than in the ferritic base metal and a steep concentration gradient. During shutdown, as temperature and hydrogen pressure drop rapidly, the hydrogen tends to leave the steel. However, the hydrogen solubility is about ten times higher in the austenitic overlay than in the base metal, while its diffusivity is much slower in the austenite than in the ferrite. Thus, as the hydrogen tries to diffuse from the ferritic base metal into the austenite, it tends to accumulate at the weld overlay interface [1]. Clearly, as the operating temperature and hydrogen pressure in the reactor are raised, the concentration of hydrogen dissolved in the reactor wall during operation increases. This increases the possibility of interface disbonding. On the other hand, a lowering of cooling rate during the shutdown practice reduces the quantum of hydrogen buildup at the interface and hence also the possibility of disbonding [9]. The composition of the base metal also exerts an influence on the susceptibility to disbonding. For example, it has been shown that the addition of vanadium to Cr-Mo steel significantly reduces the susceptibility by lowering the diffusion coefficient of hydrogen and also causing the absorption of hydrogen. The vanadium-containing precipitates can thus act as hydrogen traps and decrease the hydrogen accumulation at the weld interface [9, 10]. A common procedure to assess the disbonding tendency by laboratory testing is to introduce hydrogen into the cladding by cathodic charging or by exposure in an autoclave under specific hydrogen pressure, temperature and time conditions. On cooling to room temperature the development of disbonding, if any, is evaluated using ultrasonic testing and metallographic examination [11].

The current paper describes the application of electroslag strip cladding of austenitic stainless steel overlays on a low-alloy Cr-Mo steel base metal for use in a hydroprocessing reactor. In addition to establishing appropriate overlay and PWHT procedures, the work also involved detailed microstructural characterization.

## Experimental Work

The base material was a 55 mm thick plate of SA387 Gr11 Cl2 steel received in the normalized, accelerated cooled and tempered condition. Cladding was performed using both the single-layer and double-layer techniques. In the former, the electrode strip ~EQ309LNb was used to deposit a single layer. For the double-layer technique, the first layer employed ~EQ309L strip electrode which was followed by ~EQ347 for the second layer. The chemistries of the parent metal and the electrode strips are listed in Table 1.

**Table 1:** Chemical composition of parent metal and strip electrodes (weight%)

Elements	Base metal	~EQ309LNb	~EQ309L	~EQ347
<b>C</b>	0.13	0.008	0.005	0.012
<b>Si</b>	0.52	0.15	0.23	0.31
<b>Mn</b>	0.56	1.70	1.68	1.69
<b>P</b>	0.003	0.011	0.012	0.017
<b>S</b>	<0.001	0.0006	,0.0005	0.01
<b>Cr</b>	1.38	21.19	21.07	19.69
<b>Ni</b>	0.16	10.98	11.22	10.48
<b>Mo</b>	0.56	0.1	0.13	0.08
<b>Nb</b>	0.001	0.52	--	0.45
<b>Cu</b>	0.14	0.045	0.048	0.055
<b>N</b>	--	0.037	0.036	0.037

**Table 2:** Strip cladding conditions

<b>Current</b>	DCEP, 1050 A -1150 A
<b>Voltage</b>	25 V
<b>Travel speed</b>	170 mm/min
<b>Electrode extension (Stick out)</b>	35 mm max.
<b>Height of flux</b>	15 mm min.
<b>Preheat temperature</b>	125 <sup>0</sup> C min.
<b>Interpass temperature</b>	200 <sup>0</sup> C max.

Strip cladding was performed, depositing three weld passes side by side with 6-7 mm overlaps using the welding conditions given in Table 2. After depositing the third pass, the clad plate was heated to 300<sup>0</sup> C and kept for 3 h for dehydrogenation. After cooling down to room temperature, the weld deposit was inspected with liquid penetrant and ultrasonic examination as per ASTM A578. Ferrite measurement was done on the top surface with Fisher Ferritescope. Postweld heat treatment was carried out at 700<sup>0</sup> C for 16 hours. Although under the ASME Section VIII Div. I postweld heat treatment for only 2h 30 min is required, the longer PWHT was performed for the procedure qualification to account for possible subsequent repair welding, additional forming operations, etc.

Chemical analysis of the clad was conducted at various heights from the fusion boundary. Detailed metallographic examination of the weld interface and the cladding was also performed at different locations from the fusion line to the cladding both before and after PWHT. Aquaregia was used

as the etchant on the stainless steel side and nital on the base metal side. Microhardness survey across the weld interface was carried out before and after PWHT at different locations. Side-bend tests were performed as per ASME Section IX and intergranular corrosion test as per ASTM A 262.

Hydrogen disbonding susceptibility was evaluated in accordance with the standard procedure prescribed under ASTM Designation: G 146 – 01. The clad blank after fabrication and postweld heat treatment for 700<sup>0</sup> C for 16 h (for procedure qualification) was machined down to extract a cylindrical test specimen of 73 mm dia and 45 mm dia thickness. A stainless steel overlay was then applied to the cylindrical surface of the specimen in order to restrict hydrogen diffusion during the test to occur only in the through-reactor thickness direction, as in actual reactor service. The side overlay weld is then heat-treated 600<sup>0</sup> C for 3 h, followed by machining to prescribed dimensions. The hydrogen charging in the autoclave was performed under the test conditions – Set A (hydrogen pressure 80 bar and cooling rate 100° C/h). The details are given in Table 3. A second hydrogen disbonding test was also conducted using a higher cooling rate, but at a reduced hydrogen pressure similar to the conditions in actual service. This was performed on a second clad blank which was given a PWHT at 700<sup>0</sup> C for 7.5 h. A stainless steel overlay was applied on the cylindrical surface as before and hydrogen charging in the autoclave was performed under test conditions – Set B (hydrogen pressure 54 bar and cooling rate 150° C/ h).

**Table 3:** Test conditions for hydrogen disbonding susceptibility (autoclave method)

	Test conditions, set A	Test conditions, set B
Hydrogen pressure	80 bar	54 bar
Temperature	454° C	454° C
Holding time	48±1 h	48±1 h
Cooling rate	100° C/ h	150° C/ h
Holding time days	24±2.5° C, 168 h (7 days)	24±2.5° C, 168 h (7 days)

After completion of cooling, the specimens were removed from the autoclave and evaluated for disbonding, if any, using ultrasonic testing combined with metallographic examination.

## Results

### As-welded microstructures

The microstructure of the weld interface of the single-layer cladding using ~EQ309LNb strip electrode is shown in given in Fig. 2. This is in the form of a taper section in which the top surface of the specimen makes a small angle with the weld interface so that the width of any interface feature is magnified. The micrograph shows a transition layer between the bulk weld metal at the left and the base metal on the right. The microstructure in the transition zone was identified to be martensitic as discussed later. The micrographs of the bulk weld metal cladding at 1 mm, 2 mm and 3 mm from the interface are reproduced in Fig. 3 a, b and c, respectively. The etchant used reveals predominantly the ferrite distribution in the austenite matrix and it may be observed from Fig. 2 and 3 that the mode of solidification as well as the ferrite content changes as one moves from the weld interface into the overlay.

The double-layer cladding (309L followed by 347) exhibited features similar to the above at the weld interface and in the bulk cladding in the first layer. Fig. 4 is a micrograph of the clad metal taken at a region where the second layer (347) was deposited on the first layer (309L). The structure of the second- layer was uniform throughout and exhibited a primary ferritic solidification mode.

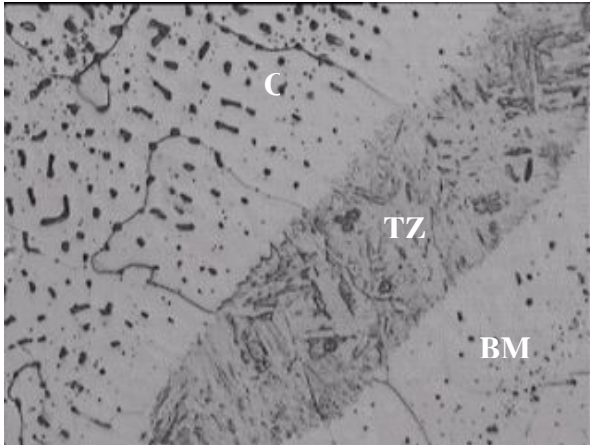


**Fig. 2 :** Weld interface in single-layer cladding showing a transition zone, as-welded  
Etchant : Aquaregia for the cladding.  
Taper section, 400X.  
BM : Base metal; TZ : Transition zone; C : Cladding



**Fig. 3a :** Bulk weld metal, 1 mm from the clad interface  
Etchant : Aquaregia. Taper section, 400X

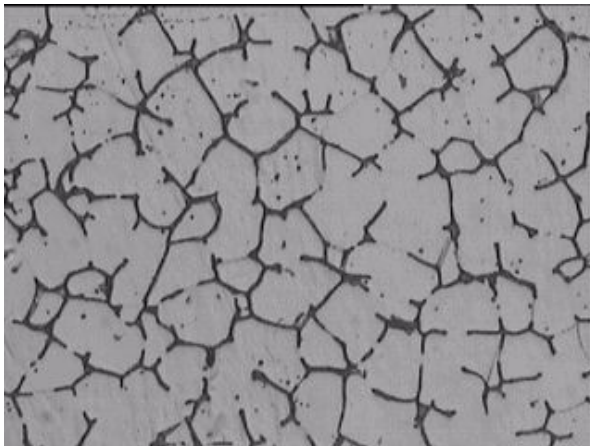


**Fig. 3b :** Bulk weld metal, 2 mm from the clad interface  
Etchant : Aquaregia. Taper section, 400X

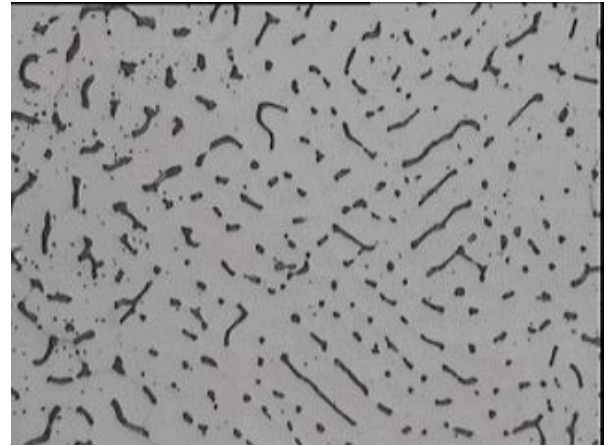


**Fig. 3c :** Bulk weld metal, 3 mm from the clad interface  
Etchant : Aquaregia. Taper section , 400X

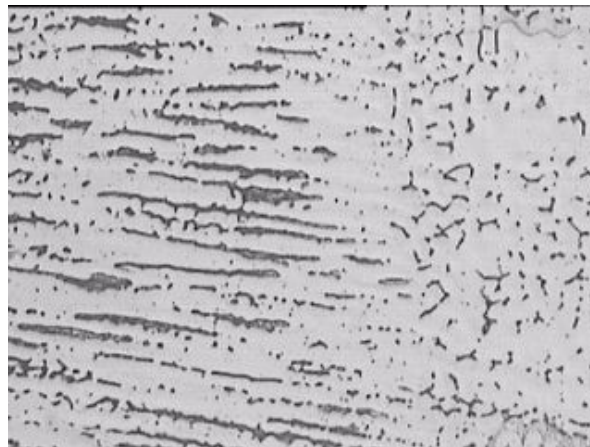


**Fig. 4 :** Micrograph of double-layer cladding at region where the second layer is deposited on the first layer. Etchant : Aquaregia, 200X  
Second layer at left, first layer at right

## Postweld heat treated microstructures

During postweld heat treatment for 16 h at 700<sup>0</sup> C, several diffusion-based reactions occur in the cladded joint, especially at and near the weld interface. Fig. 5 is a micrograph of the interface region after PWHT in the single-layer overlay. It shows a heavily dark-etching layer marking the transition zone between the base metal and bulk weld metal. This was the region which exhibited a martensitic structure in the as-welded condition (Fig.2) and in which considerable carbide precipitation has occurred during PWHT. Next to this layer on the clad metal side is a region of weld metal showing the total absence of ferrite. This fully austenitic region is bounded on the other side by a grain boundary running approximately parallel to the dark-etching layer and the weld interface. This grain boundary has been referred to in the literature as a 'Type II boundary' [8, 12] and is discussed below. Further into the weld metal on the left of the Type II boundary is the more usual austenitic weld metal structure containing ferrite in the substructure boundaries within the austenite grains. The boundaries of these austenite grains represent the conventional or Type I grain boundaries.

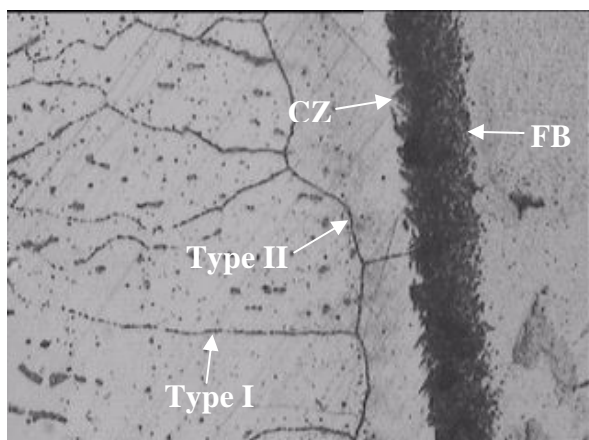


**Fig. 5 :** Weld interface in single-layer cladding after PWHT, Etchant : Aquaregia, 400X  
Note the presence of a carburized zone and Type II grain boundary. Type I and Type II grain boundaries are indicated by arrows.  
FB: Fusion boundary; CZ : Carburized zone.

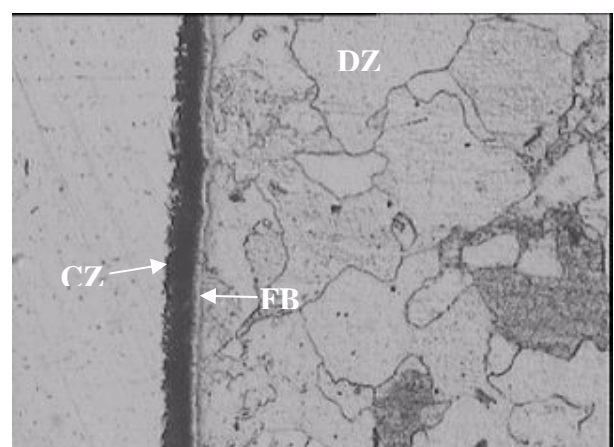


**Fig. 6 :** Base metal region adjoining weld interface after PWHT in single-layer cladding.  
Note presence of the decarburized, coarse ferritic region (DZ)  
Etchant : Nital, 200X.

Fig. 6 on the base metal side of the dark-etching interface layer exhibits a nearly totally decarburized base metal structure. Note also that the ferrite grains here are able to grow to large sizes in the absence of the carbide phase. It is surmised that carbon in this region has diffused from the base metal toward the overlay because of the concentration gradient and its affinity for the higher Cr content in the clad metal.

## Microhardness

The microhardness distributions across the weld interface both in the as-welded condition and after PWHT are plotted in Fig.7. In the as-welded condition, there is a moderate increase in hardness at the weld interface region, which can be attributed to the formation of a low-carbon martensite. After postweld heat treatment the hardness of this region registers a significant increase, presumably as a result of heavy carbide precipitation. On the base metal side of the interface after postweld heat treatment, there is a noticeable softening effect as a result of the migration of carbon from this region to the interface.

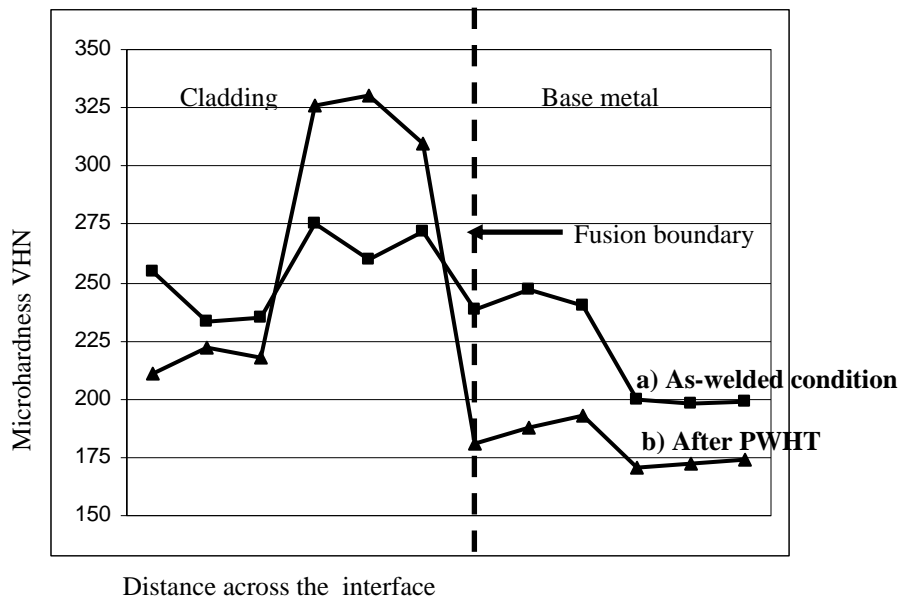


**Fig. 7 :** Microhardness distributions across clad interface

### Composition gradients

The chemical analyses of the bulk weld metal in the single-layer overlay at 2.5 mm, 3 mm and 3.5 mm from the fusion boundary are given in Table 4. These show a relatively uniform composition in the bulk cladding, corresponding to the strip electrode mixed with the base metal to an average degree of dilution depending on the welding parameters. However, as the base metal is approached, there are steep concentration gradients in the interface region that includes the transition zone described above. Scanning electron microscopy EDS analyses of the interface region both in the as-welded and postweld heat treated condition are listed in Table 5.

**Table 4:** Chemical analysis of single-layer overlay in the bulk weld metal

	Location From Fusion Line to Overlay		
	2.5 mm ←	3.0 mm	3.5 mm →
<b>Elements</b>	<b>Weight%</b>		
Carbon	0.022	0.022	0.024
Manganese	1.11	1.01	1.01
Silicon	0.28	0.2	0.192
Chromium	18.11	18.14	18.56
Molybdenum	0.17	0.2	0.17
Nickel	9.34	9.53	9.46
Niobium	0.32	0.35	0.34

**Table 5 :** EDS (SEM) chemical analysis in the interface transition zone in single-layer overlay

Description	%Cr	%Ni
As-welded, location 1	3.23	1.61
As-welded, location 2	3.51	1.42
After PWHT, location 1	13.44	5.17
After PWHT, location 2	11.66	4.02

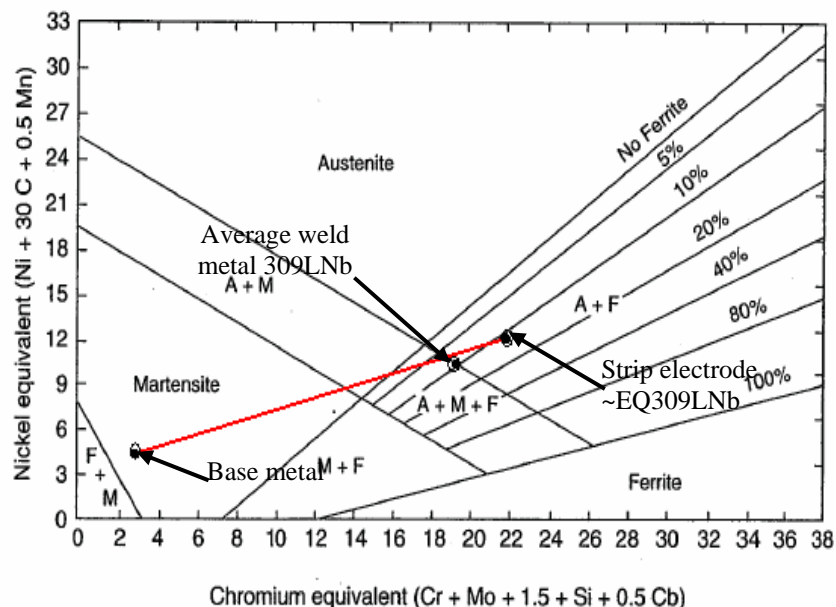
## Discussion

### Microstructural characterization

The evolution of microstructure during cladding and during subsequent postweld heat treatment offers many features of metallurgical interest, which must be understood for assessing the service behavior of the cladded joint. There are structural changes occurring in the base metal close to the weld, at the weld interface itself and in the bulk weld metal. In the present case, near the top and in the bulk clad metal, the composition approximates to that of the strip electrode, modified by the average dilution, but near the weld interface there are significant composition gradients produced due to a combination of dilution and other factors which have a profound effect on the microstructural development

The changes in composition and microstructure across the transition zone at the weld interface are of particular importance because this is where possible hydrogen disbonding can occur in service. While the dilution level in the bulk weld metal under ESSC conditions is known to be not more than about 15%, near the fusion boundary the degree of dilution will be much higher. This is most likely to be the result of the formation of a stagnant fluid layer in the weld pool adjacent to the base metal. The transition from the low alloy content (Cr, Mo) in the base metal to the high alloy content (Cr, Ni, Nb) in the bulk weld metal occurs in this transition zone. The layer originally had the same composition as the base metal, but develops higher chromium and nickel contents as a result of diffusion from the cladding due to the concentration gradients [13]. The stagnation layer has also been called the unmixed zone [14]. It may be seen from Table 5 that Cr contents over 3 % and Ni contents around 1.5 % could develop in the transition zone during cladding. The composition in the layer is such that during cooling following overlaying this region transforms to martensite.

The change in composition from the base metal to the bulk weld metal through the transition zone can also be understood from the Schaeffler diagram, Fig.8. A tie-line is drawn on the Schaeffler diagram connecting the base metal to the strip electrode composition corresponding to 309LNb. It can be seen that, depending on the local dilution level in the weld metal, intermediate compositions can develop martensitic or austenitic-martensitic microstructures. As seen above, the local dilution level in the transition zone next to the fusion boundary can be much higher than in the bulk clad metal farther away. It is thus clear that in the as-welded condition the transition zone will exhibit a partially or wholly martensitic microstructure.



The microhardness measurement taken across the weld interface in the single-layer procedure reveals (Fig.7) a significant hardness increase in the as-welded interface region, thus confirming the presence of martensite. The hardness of the martensite would strongly depend on the local carbon

content. It may be noted that, although the filler material carbon content is very low (0.008%), some carbon might be picked up from the base metal. The carbon content in the latter is 0.13%. This means that the martensite in the transition region is likely to have a carbon content well below 0.1%, which accounts for the fact that the interface martensite exhibits only a moderate hardness (~275 HV).

The microstructures in the weld interface region in the single-layer overlay after postweld heat treatment exhibit several features of interest. Fig.6 reveals a zone in the base metal adjoining the fusion boundary, about 10  $\mu\text{m}$  wide, in which there is heavy decarburisation and a structure that is nearly fully ferritic. Correspondingly, Fig. 5 and Fig. 6 show a thin dark-etching layer on the weld metal side of the fusion boundary. It should be noted that this was the region of the transition zone which in the as-welded condition exhibited a martensitic condition. During the long postweld heat treatment for 16 h at 700°C, carbon tends to diffuse from the base metal into the cladding on account of the difference in carbon contents: the base metal had 0.13% C, and the bulk weld metal ~0.02% C. The carbon migration is also aided by the fact that chromium content in the clad is far higher than that in the base metal. The migrated carbon forms chromium carbide ( $\text{Cr}_{23}\text{C}_6$ ) (and also NbC in the present case since ~EQ 309LNb was used) at the weld interface. As the carbon thus leaves the base metal, a carbon-depleted zone is formed adjacent to the fusion boundary, Fig. 6. Such decarburized zones are known to form in heat-treated ferritic-austenitic welds and the subject is well documented [15-17]. The microhardness survey (Fig. 7) also shows a hardness reduction corresponding to the decarburized region.

The microhardness distribution further reveals that as a result of the postweld heat treatment the hardness of the transition region has increased to as high as ~330 VHN, which is significantly higher than the ~275 VHN measured here in the as-deposited condition. Thus, although a PWHT at 700°C tempers the martensite, the hardness still rises to a high value. An explanation for this is to be found in the diffusion of carbon from the base metal to the interface region during the 16 h-long treatment at 700°C. The carbon then combines with the chromium already present in the transition region (and also with Nb when ~EQ309LNb strip is used). In fact, it is further likely that more Cr and Nb would also diffuse to the interface zone from the bulk clad metal, the driving force being the affinity for carbon migrating to the same region from the base metal. The scanning electron microscope EDS analysis of the transition zone (Table 5) shows that after PWHT the Cr content here could rise to a level > 10 %. Thus, there is considerable alloy carbide formation at the weld interface region during prolonged PWHT. This in fact accounts for the dark-etching behavior of the interface layer (Fig.5). In addition to the carbide precipitation, it has been suggested that fresh martensite could also form during cooling from the PWHT temperature [1]. It has also been demonstrated that double PWHT procedures can be developed to decrease the hardness of the interface region by tempering the martensite formed during cooling from the first PWHT temperature [18]. The hardness increase at the weld interface due to PWHT is to be attributed to these reasons.

The weld metal micrographs in the single-layer cladding at different distances, viz., 1mm, 2 mm and 3 mm from the interface are reproduced in Fig.3 a, b and c, respectively. It may be noted in Fig. 2 that the weld metal immediately adjoining the transition zone contains virtually no ferrite and solidification has occurred fully as austenite. As one moves away from the interface, primary solidification is still austenitic, but the remaining liquid between the dendrites solidifies as ferrite. Traversing into the bulk cladding, as seen in Fig. 3a, the solidification mode changes from primary austenitic to primary ferritic, both types being visible in Fig.3a. On the other hand Fig. 3b shows totally skeletal or vermicular ferrite, the ferrite being the primary phase forming at the core of the dendrites. This trend continues in Fig. 3c, 3 mm away from the interface, which is also vermicular but somewhat coarser than Fig. 3b.

For the bulk 309LNb weld metal (corresponding to the average composition listed in Table 4), the average ferrite content estimated from the Schaeffler diagram is 7-8%. However, the dilution level increases significantly in the transition zone at the weld interface. The carbon concentration in this region is considerably higher than in the bulk weld metal because of the carbon migrating from the base metal. This carbon tends to accumulate at the interface without migrating further into the cladding since the diffusion coefficient of the carbon in austenite is very low [2]. The carbon accumulated at the interface results in fully austenitic weld metal solidification in the cladding adjacent to the interface.

On moving away from the weld interface into the bulk cladding, more and more ferrite forms during solidification. Thus, at 1 mm from the weld interface (Fig. 3 a), there is primary austenite solidification. At 2 mm (Fig. 3 b) and 3 mm (Fig. 3 c) from the interface, the solidification mode becomes primary ferritic and the ferrite content also increases to reach a level corresponding to the average cladding composition.

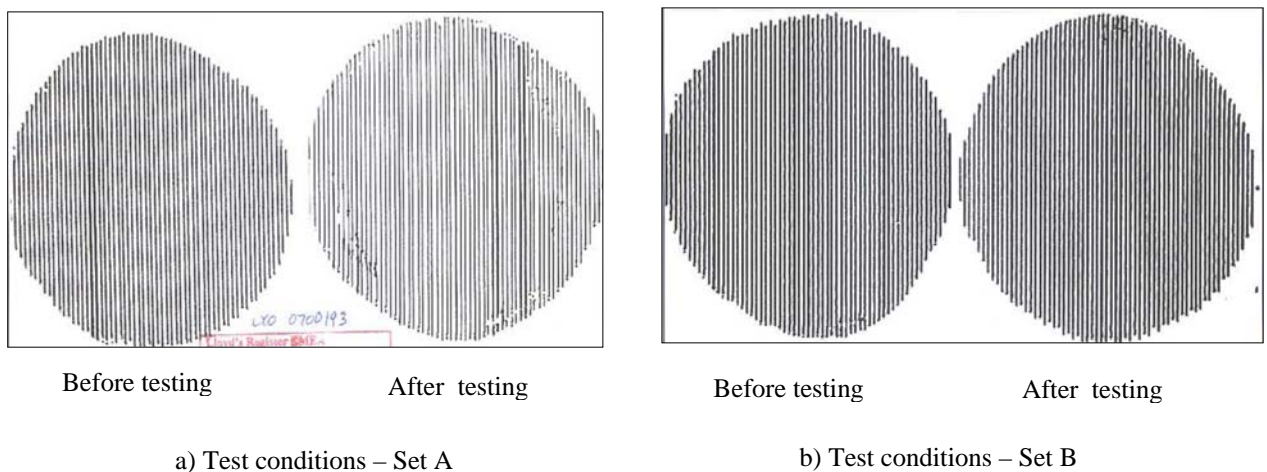
Fig. 4 is a micrograph of the double-layer cladding taken at region where the second layer (347) was deposited on the first layer (309L). Throughout the second layer, from the region shown in Fig. 4 to the top of the cladding, the weld metal has solidified in the primary ferritic mode, exhibiting a vermicular ferritic structure. It may be noted that the dilution level and hence the composition are nearly the same throughout the second layer of the cladding, so that there is no change in solidification mode, which remains primary ferritic throughout.

Fig. 5, which illustrates the weld interface region in a single-layer overlay after PWHT, exhibits the so-called Type II boundary running roughly parallel to the weld interface. Weld metal solidification usually occurs by epitaxial nucleation along the fusion boundary, giving rise to grain boundaries in the fusion zone that are roughly perpendicular to the fusion boundary [12]. These have been referred to as type I boundaries and they occur when crystal structures of the weld metal and base metal are the same. On the other hand, when the weld metal is austenitic and the base metal ferritic, normal epitaxial nucleation cannot occur and hence the austenite is forced to nucleate heterogeneously from the fusion boundary[19]. This results in the formation of Type II boundaries as shown in Fig. 5. The more commonly observed Type I boundaries are also indicated in the figure.

### Quality assessment tests

Dye-penetrant and ultrasonic testing of both the single-layer and double-layer overlays revealed no defect indication. Similarly, side-bend tests as per ASME Section IX also confirmed the soundness of both types of claddings. For the intergranular corrosion tests as per ASTM A 262 Practice 'E', the bent area was found to be free from any IGC fissure or crack in all the overlays.

The results of the hydrogen disbonding tests employing hydrogen charging in an autoclave were also entirely satisfactory. Fig. 9a and Fig.9b show the ultrasonic scans of the two test specimens. It may be observed that no disbonding indication is visible in either of the scans and no disbonded area could be observed. For comparison, Fig. 9c shows an ultrasonic scan of a hydrogen-charged specimen (taken from the literature) showing a disbonding defect. It is clear from Fig. 9a and 9b that the overlay joints in the current investigation did not contain any disbonded area.



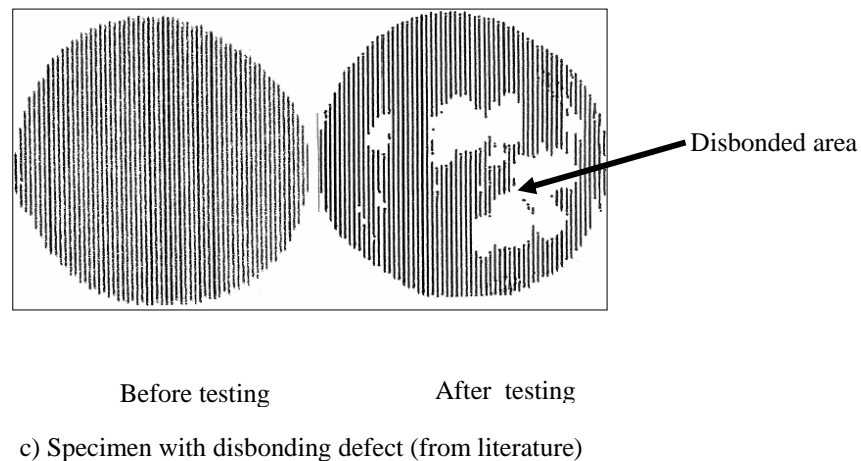


**Fig. 9 :** Ultrasonic scans before and after hydrogen charging in autoclave

Another potentially important result from the present study is that single-layer overlays may be expected to perform in reactor service just as satisfactorily as double-layer overlays. Table 4 shows that the composition near the top of the single layer cladding, indicating C, Cr and Ni contents to be 0.024%, 18.56%, and 9.46%, respectively. The corresponding values near the top of the double-layer cladding in the current work were 0.022% C, 19.38% Cr, and 10.32% Ni. The Cr and Ni contents in the single-layer overlay are understandably slightly lower than in the double-layer overlay on account of the higher dilution effect. However, the difference is of a very low magnitude, indicating that the single-layer cladding itself might provide acceptable quality for reactor service. It is worthwhile to do further work and establish the reliability of single-layer overlays in view of their obvious economic advantage.

## Conclusion

1. Electroslag strip cladding can be advantageously and profitably used to deposit austenitic stainless steel overlays on low-alloy steel base metal.
2. During cladding and during postweld heat treatment, structural changes occur especially in the weld interface region, which result in a carbon-depleted zone in the base metal and a carbon-enriched (alloy carbide) layer in the weld metal next to the interface.
3. The weld interface region could be a potential location for hydrogen disbonding during service, but in the overlays produced in the current work, no such disbonding susceptibility could be detected.
4. Other quality assessment tests also demonstrated the entirely acceptable joint quality.
5. Preliminary indications are that single-layer overlays, which are obviously more economically attractive, might provide acceptable quality for reactor service. Further work is needed, however, to establish their reliability.

## Acknowledgement

The current work constitutes the project work of Mitul Patel in the L&T-sponsored M.E. (Welding Technology) programme at the Dept. of Met. & Matls. Engg., M .S. University, Vadodara. The contribution of Larsen & Toubro Ltd. and the Department faculty is gratefully acknowledged.

## References

1. R. Paschold, L. Karlsson and M. F. Gittos, Svetsaren, 1 (2007) 10-15.
2. Y. K. Oh, J. H. Devletian and S. J. Chen, Welding Journal, 69 (1990) 1, 37-40.
3. G. Gallazzi, S. Rigdal and M. Kubenka, Svetsaren, 1 (2007) 17-22.
4. J. H. Devletian, Y. P. Gas, Q. H. Zhao and W. E. Wood, NSRP Ship Production Symposium, Society of Naval Architects and Marine Engineers, New Orleans, USA, 1997, 7C2-1 to 7C2-2
5. S. G. Forsberg, Welding Journal, 64 (1985), 41-48.
6. H. Heuser, Thyssen Schweisstechnik, GmbH, Germany.

7. S. Nakano, N. Nishiyama, T. Hiro, J. Tsuboi, Kawasaki Steel Technical Report No. 2, March 1981.
8. T. W. Nelson, J. C. Lippold and M. J. Mills, *Welding Journal*, 79 (2000) 11, 267s-276s.
9. J. Shimomura, Y. Nakano, S. Nakano and S. Veda, *ISIJ International*, 31 (1991) 4, 379-386.
10. F. Fusari et al, *Welding in the world*, 36 (1995), 173-180.
11. ASTM Designation G 146 – 01, Dec. 2001.
12. M. D. Rowe, T. W. Nelson and J. C. Lippold, *Welding Journal*, 88 (1999) 2 , 31s - 37s.
13. Y. K. Oh and J. H. Devletian, *Welding Journal*, 71 (1992), 37-44.
14. W. F. Savage, E. F. Nippes and E. S. Szekeres, *Japan Welding Society* 43 (1976) 2, 162-173..
15. C. D. Lundin, *Welding Journal*, 61 (1982) 2, 58s – 63s.
16. K.G.K. Murti and S. Sundaresan, *Welding Journal*, 64 (1985) 12, 327s – 334s.
17. M. Sireesha, S. K. Albert and S. Sundaresan, *Welding Journal*, 79 (2002), 819 – 827.
18. S. Pak, S. Rigdal, L. Karlson, A. Gustavsson, *ESAB Svetsaren*, 51(1996)3, 28-33
19. J.C. Lippold, D. J. Kotecki, *Welding Metallurgy and Weldability of Stainless Steels*, Wiley Interscience, USA, 2005.